



OPEN ACCESS

EDITED BY

Qiuming Pei,
Southwest Jiaotong University, China

REVIEWED BY

Gang Zhang,
Southwest University of Science and
Technology, China

Dewei Li,
China Geological Survey, China
Gang Min,
Chengdu University of Technology,
China

*CORRESPONDENCE

Qiao Wang,
✉ 540363176@qq.com

SPECIALTY SECTION

This article was submitted to Structural
Geology and Tectonics,
a section of the journal
Frontiers in Earth Science

RECEIVED 05 January 2023

ACCEPTED 06 February 2023

PUBLISHED 22 February 2023

CITATION

Wan H and Wang Q (2023), Electrical
structure of Gulu geothermal field in
Southern Tibet and its implication for the
high-temperature geothermal system.
Front. Earth Sci. 11:1138360.
doi: 10.3389/feart.2023.1138360

COPYRIGHT

© 2023 Wan and Wang. This is an open-
access article distributed under the terms
of the [Creative Commons Attribution
License \(CC BY\)](https://creativecommons.org/licenses/by/4.0/). The use, distribution or
reproduction in other forums is
permitted, provided the original author(s)
and the copyright owner(s) are credited
and that the original publication in this
journal is cited, in accordance with
accepted academic practice. No use,
distribution or reproduction is permitted
which does not comply with these terms.

Electrical structure of Gulu geothermal field in Southern Tibet and its implication for the high-temperature geothermal system

Hanping Wan¹ and Qiao Wang^{2*}

¹Beijing Research Institute of Uranium Geology, Beijing, China, ²China Geological Survey, Chengdu Centre, Chengdu, China

The Yadong-Gulu rift (YGR) South Tibet is a Cenozoic active rift, which is endowed with abundant geothermal resources. The Gulu geothermal field (GGF) is located in the Northern section of the rift, where a large number of high-temperature hot springs develop, but its geothermal system is mysterious. In this study, the three-dimensional (3D) electrical structure of GGF is revealed by broad magnetotelluric (MT) and audio magnetotelluric (AMT). MT reveals that middle and upper crust conductors are developed in the subsurface of GGF. The conductors may originate from the partial melting that drives the geothermal system. AMT reveals that the electrical structure of GGF is conductive alternation cap overlying more resistive reservoir, which is consistent with the classical electrical structure of geothermal systems in worldwide active tectonic zones. According to the geothermal system model, cold fluids may converge from the periphery of GGF to the middle, wherein fault F1 (the Western branch of Jiulazi-Sanxung fault) may be the main channel for cold fluids to migrate downward. The fluids are heated by partial melting in the middle and upper crust, and may migrate upward along fault F2 (the middle branch of Jiulazi-Sanxung fault) and develop into heat reservoirs.

KEYWORDS

magnetotelluric, audio magnetotelluric, Gulu geothermal field, geothermal system model, electrical structure

1 Introduction

The YGR in the Southern Tibet is a Cenozoic active rift, which is characterized by active normal faults, frequent earthquakes, widespread thermal springs and high terrestrial heat flow, being endowed with abundant geothermal energy (Armijo et al., 1986; Hu et al., 2000; Yin and Harrison, 2000; Wu et al., 2011; Chevalier et al., 2020; Bian et al., 2022), Figure 1. High-temperature geothermal energy is renewable and can be used for power generation (Barbier, 2002; Rybach, 2010). The only two commercial geothermal power stations in China are located in the middle of YGR, that is Yangbajing geothermal field and Yangyi geothermal

Abbreviations: CSR, Cona-Sangri rift; GGF, Gulu geothermal field; JF, Jiali fault; MFT, Main front thrust; NS, Bangong-Nujiang Suture; PXR, Pumqu-Xainza rift; TYR, Tangra-Yumco rift; YGR, Yadong-Gulu rift; YZS, Yarlung-Zangbo suture.

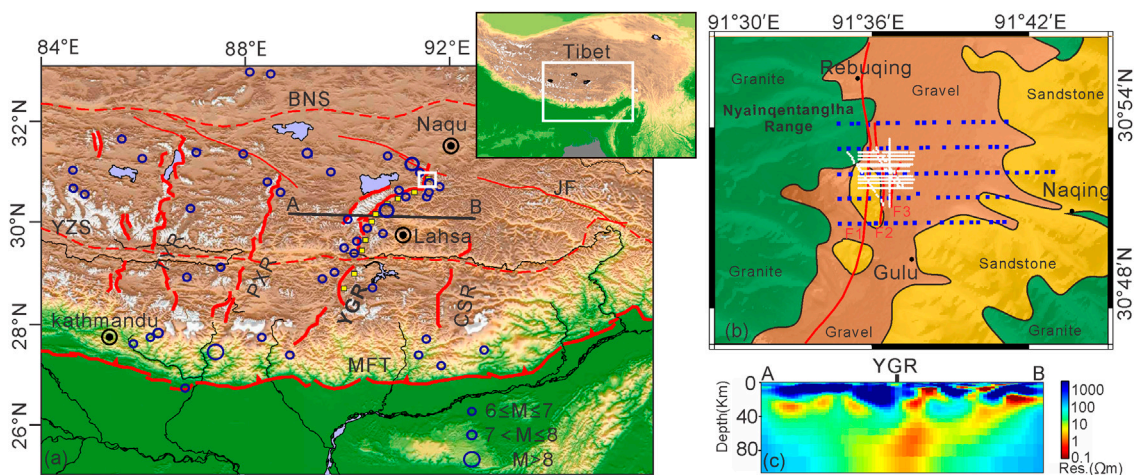


FIGURE 1

Geologic setting and sounding sites (A) Tectonic framework of Yadong-Gulu rift (modified from Shi et al., 2020). A large number of earthquakes are distributed around YGR, suggesting that YGR has intense activity. Red dots are faults. Blue circles are earthquakes. Yellow diamonds are geothermal manifestations. Black line is the previous MT section, as shown in Figure 1C. (B) Sounding sites overlap on the geology of Gulu geothermal field. Jiulazi-SanXung fault is consist of fault F1, F2 and F3. Nyainqentanglha Range is mainly composed of granite. The middle Jurassic Mali formation sandstone (J_2m) and Quaternary gravel (Q) are the sedimentary strata of GGF. Blue diamonds are MT sites. White dots are AMT sites. (C) Electrical model of section AB (modified from Wang G et al., 2017). High conductors of mantle origin are distributed in the subsurface of YGR.

field, whose installed capacity is 25.15 MW and 16 MW, respectively (Dorji, 2003; Wang and Guo, 2010). A large number of high-temperature hot springs are developed on the surface of GGF, which is located in the north of YGR (Liu et al., 2014), Figure 1A. The unclear geothermal system of GGF limits the development of commercial power generation.

Geothermal systems are generally composed of shallow structures and deep heat sources, the former is key to understand geothermal systems (Cumming, 2009; Liao, 2017). Water geochemistry indicates that atmospheric precipitation is the main source of groundwater, including a small amount of magmatic water (Liu et al., 2014; Su et al., 2020; Wang et al., 2020; Yu et al., 2022). Tensional faults constitute fluid circulation channels and thermal reservoirs (Zhang et al., 2014; Wang S et al., 2017). The Quaternary hydrothermal sinter seals off the geothermal reservoirs, and the widely distributed hot springs imply good geothermal potential (Gao et al., 2022). The north-south active normal fault obviously controls the hydrothermal activity (Li and hou, 2005; Wu et al., 2006; Guo et al., 2007). Previous studies on the formation mechanism of geothermal system are mainly based on surface investigation (Zhao et al., 2002; Liu et al., 2009; Feng et al., 2012; Hu et al., 2022), laying a foundation for understanding of GGF geothermal systems. However, the lack of deep structure seriously restricts the understanding of GGF geothermal system.

Electrical resistivity in the subsurface is sensitive to characterize geothermal context, such as the shallow geothermal structure and deep heat source (Newman et al., 2008; Muñoz, 2013; Spycher et al., 2014). Fluid-bearing faults (or fractures) and heat sources are the main components of geothermal systems, which often show high conductivity and are easy to be imaged by MT (Abiye and Haile, 2008; Piña-Varas, et al., 2014; Peacock et al., 2016; Paolo et al., 2020). In this study, MT and AMT imagining have been carried out, and 3D inversion has been implemented to obtain the electrical structure

of the middle and upper crust of GGF. Combining with previous researches, the origin of heat source is discussed on the electrical structure of MT. This study reveals the distribution of shallow geothermal systems by AMT. On this basis, the geothermal systems in tectonically active zones around the world are compared and analyzed, and the geothermal system model of GGF is constructed, which provides an important basis for understanding the geothermal system model of YGR in the South Tibet.

2 Materials and methods

To clarify the origin of deep heat source in the GGF, we deployed 3D MT. The space of MT sites is about 0.6 km, and the collecting time is about 24 h with five components of electromagnetic field (Ex, Ey, Hx, Hy, Hz). In addition, in order to understand the fault and fluid distribution, 3D AMT was carried out in the hot springs developed area. The AMT space is about 0.05 km, the collecting time is 1 h with 5 components of electromagnetic field. Both MT and AMT data were collected by Phoenix V5-2000. On this basis, impedance tensors were estimated through the robust technique (Egbert, 1997).

The 3D inversion of MT and AMT data were carried out on the ModEM modules (Egbert, 2012; Kelbert et al., 2014). 3D inversion can effectively minimize the influence of off-profile structure and reveal a more real subsurface structure (Siripunvaraporn, 2011). Input data for the 3D inversions are all components of the MT and AMT impedance tensor for period range from 0.0001–1,000 s. The error floor for all tensors were 5% of $\sqrt{(|Z_{xy} \times Z_{yx}|)}$. The starting model was set to a uniform half space with background resistivity of 100 Ωm , which was divided in a grid of $94 \times 130 \times 80$ cells in the x, y, and z directions, respectively. In the data coverage part, horizontal

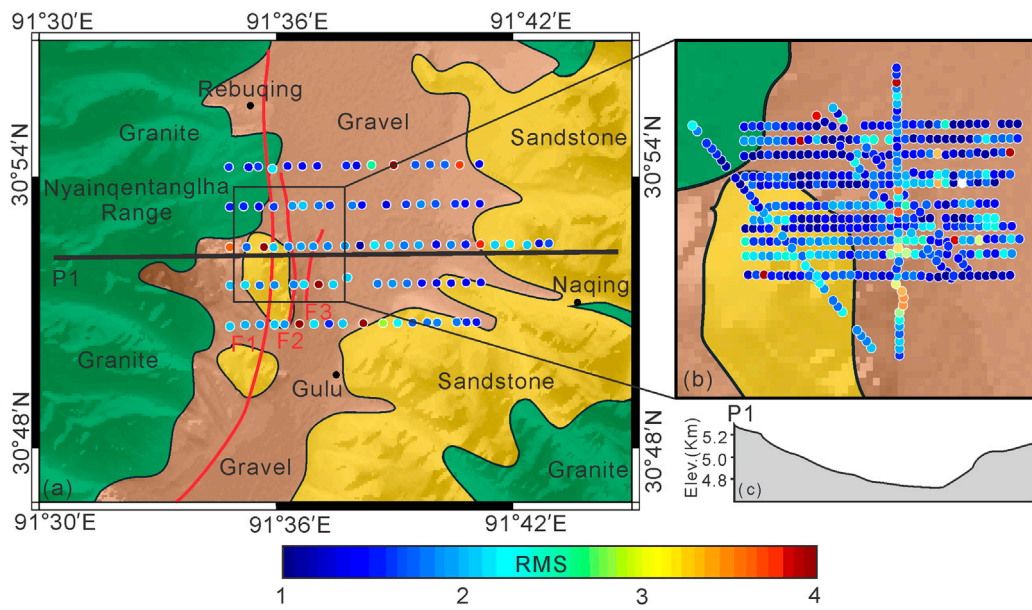


FIGURE 2
 RMS of Magnetotelluric 3D inversion and tomographic section. **(A)** RMS of MT 3D inversion. RMS of most MT sites is less than 3. **(B)** RMS of AMT 3D inversion. RMS of a few AMT sites is around 4. **(C)** Topographic section of P1. The high terrain on both sides of GGF facilitates fluid migration to the center.

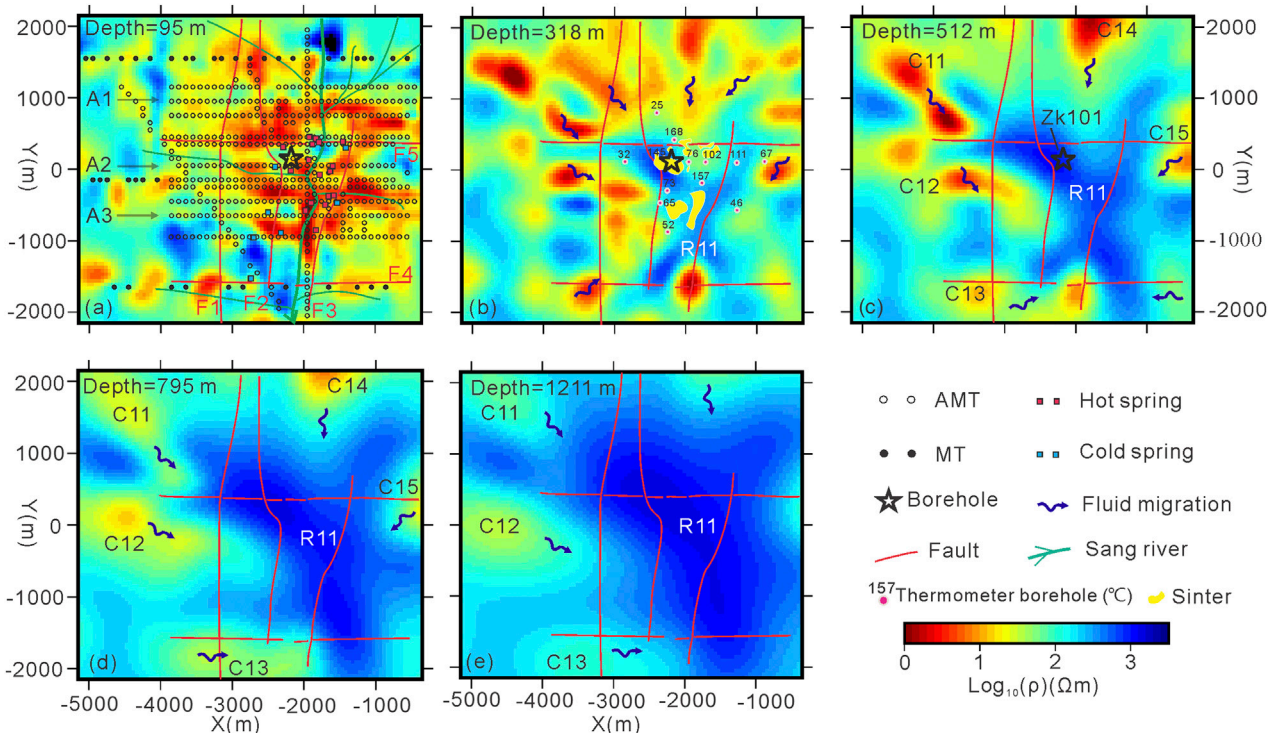


FIGURE 3
 Horizontal slices of electrical model at different depths revealed by AMT. **(A–E)** Horizontal slices at depths of 95 m, 318 m, 512 m, 795 m, 1,211 m, respectively. The electrical model has the characteristics of high conductivity in the shallow depth **(A–C)** and high resistivity in the deep depth **(D–E)**. Thermometer boreholes with depths of 57.1–83.1 m give out temperatures at the bottoms, as shown in Figure 3B.

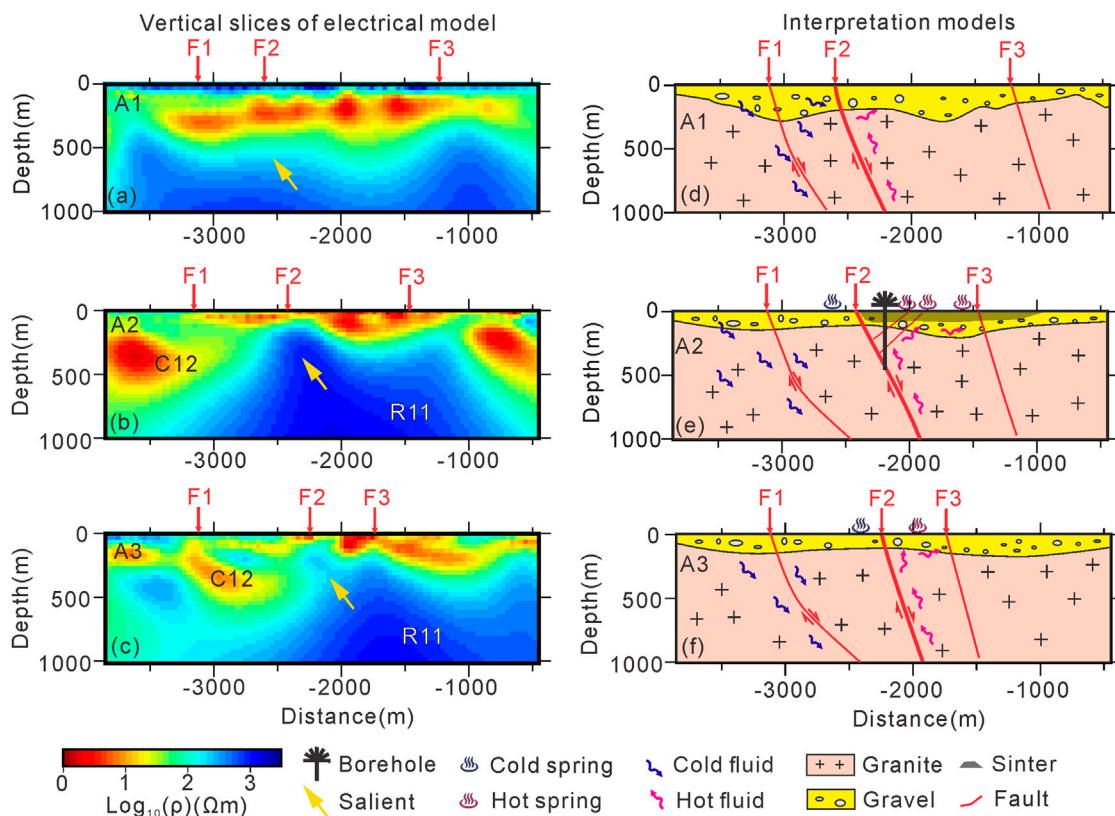


FIGURE 4

Vertical slices of electrical model and interpretation revealed by AMT. (A–C) Section resistivity models of A1–A3. High resistivity salient is an important feature in the electrical model, as shown by yellow arrows. (D–F) Interpretation models of A1–A3. Faults F1 and F2 may be the cold and hot fluids migration channel, respectively. The resistor R11 may imply presence of granite.

cell sizes are set to 0.1×0.1 km. Ten padding cells with an increasing factor of 1.5 were also included. In the vertical direction, first layer is set to 50 m thickness, followed by 79 layers increasing thicknesses gradually by a factor of 1.1. After 103 times of iteration, the root-mean-square (RMS) misfit reached 2.18 (Figure 2), and a reliable resistivity model was obtained.

3 Results

3.1 Electrical structure of shallow depth revealed by AMT

The electrical structure in shallow depth is characterized by high resistivity in the middle and high conductivity in the periphery. Geothermal systems typically consist of faults and fractures filled with geothermal fluids that may contain high concentrations of dissolved salts resulting in the presence of conductive electrolytes in the rock matrix (Muñoz, 2013). Hence, the resistivity of geothermal systems composed of fluids and electrolytes is about $n \times 10 \Omega\text{m}$ (high conductivity), and that of granites is about $n \times 100 \Omega\text{m}$ (high resistivity) (Newman et al., 2008; Peacock et al., 2012; Muñoz, 2013). These features provide an important basis for the interpretation of AMT data. Resistivity models at depths less than 0.4 km show that high conductivity ($\rho < 10 \Omega\text{m}$) is the dominant feature (Figure 3A, B),

which may be related to the Quaternary strata, faults or fluids. Resistivity models of depths greater than 0.4 km show that there is a resistor R11 ($\rho > 1,000 \Omega\text{m}$), implying the presence of granite. The conductors C11, C12 and C13 located around the resistor R11 extends below 1 km, while the thickness of Quaternary strata in this area is generally less than 0.2 km (Armijo et al., 1986). We conclude that the shallow conductors may be related to the fluid migration.

Section A3 reveals fluid migration in the GGF. Conductor C12 is distributed beneath fault F1, extending to a depth of less than 1 km, which is inferred to be the migration direction of cold fluids. The migration direction is consistent with the topographic distribution of the surface, as shown in Figure 2C. In addition, a large number of cold springs distributed near fault F1, indicating that fault F1 may be the cold fluid channel, as shown in Figure 3A. The resistivity anomaly that cannot be ignored in Figure 4 is the high resistivity salient, marked by yellow arrows. The high resistivity salient may be caused by fault F2. The fault F2 may be a deep fault that controls granite invasion and also constitutes a heat-conducting channel. Borehole ZK101 revealed 5 layers of heat reservoirs and dozens of hydrothermal alteration zones in the hanging wall of fault F2 (Gao et al., 2022). In addition, there are a large number of hot springs and sinters on the eastern side of the fault F2 (Figures 3A, B), suggesting that the fault F2 may be an important heat-conducting channel for the GGF.

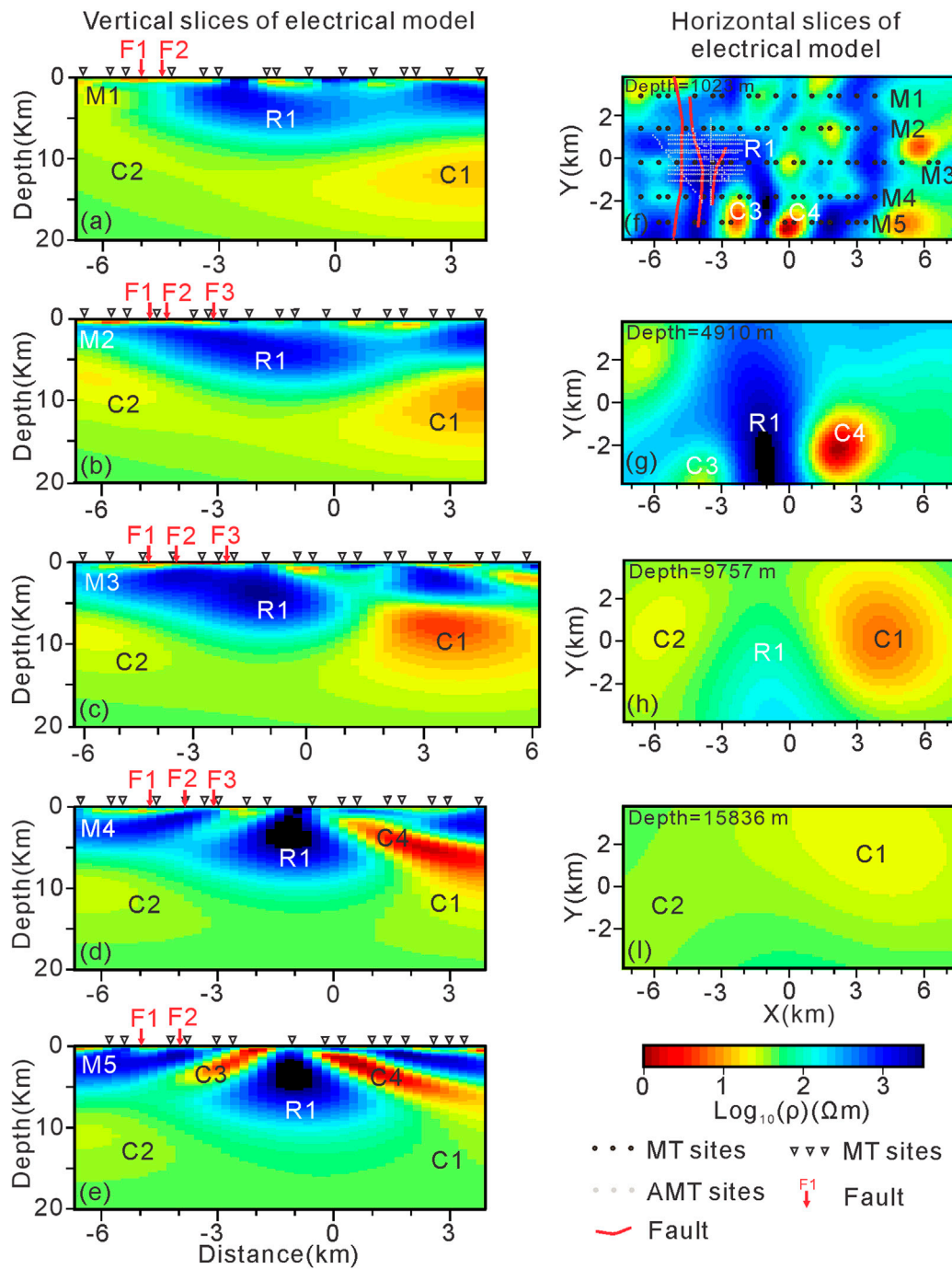


FIGURE 5
 Horizontal and vertical slices of resistivity in GGF revealed by the MT. Figure (A–E) are vertical resistivity slices of M1 - M5, respectively. The vertical models are characterized by high resistivity at depth above ~8 km and high conductivity at depth below 8 km. Figure (F–I) are horizontal resistivity slices of depths at 1,028 m, 4,910 m, 9,757 m, 15,836 m, respectively. Conductors C1 and C2 dominate the electrical anomaly of horizontal models. AMT sites indicate the location of GGF.

Different from section A2 and A3, section A1 reveals that there is a continuous and stable layer of high conductivity in the shallow depth, suggesting different geothermal context between the South and North of GGF. The nearly continuous conductivity layer in Figure 4A may suggest that there is an abundance of

subsurface fluids and even good connectivity between these fluids. The influx of cold fluid will reduce the temperature of hot fluid, which is not conducive to the exploration of high-temperature geothermal system. This may also be the main reason why there is no surface hydrothermal activity in the

north of GGF, as shown in [Figure 3B](#). Combined with surface geology, boreholes, and resistivity anomalies, we deduce the deep extension of the faults F1, F2 and F3, [Figures 4D–F](#). After clarifying the superficial fluid and fault system, it is the key to understand the deep heat source.

3.2 Electrical structure of middle and upper crust revealed by MT

The horizontal slice of 3D electrical structure is important for understanding the transverse distribution of anomalous electrical bodies. According to the 3D inversion results, the electrical structures with depths of 1,023 m, 4,910 m, 9,757 m and 15,836 m were plotted, as shown in [Figures 5A–D](#). The resistor R1 ($\rho > 1,000 \Omega\text{m}$) and the conductors C1 and C2 ($\rho < 30 \Omega\text{m}$) are distributed at different depths. Resistor R1 may represent intact granite and is an important medium for deep heat conduction to the surface ([Newman et al., 2008](#); [Piña-Varas, et al., 2014](#)). The resistor R11 in [Figure 4](#) is the shallow part of resistor R1 in [Figure 5](#) on account of the same electrical anomaly and similar resistivity value. Resistors R11 and R1 represent the nearly intact granites. In [Figure 5A](#), four conductors (C1, C2, C3, C4) are distributed around the resistor R1. They gradually become discrete on the shallow surface, which may indicate fluid migration, which has been elaborated on the AMT section. Conductors C3 and C4 are located above the R1 in [Figures 5D, E](#), implying that there might be two blind faults bearing fluids in the southern GGF ([Figures 5F, G](#)). Conductors C1 and C2, located in the either side of GGF, extend deep and are more clearly shown in the sections.

High conductivity domains the main resistivity feature in the subsurface of GGF. Conductors C1 and C2 ($\rho < 30 \Omega\text{m}$) has been imagined in these sections, among of which the section M3 is representative, [Figure 5C](#). Section M3 shows different conductivity anomaly at the east and west of GGF. The west is characterized by resistivity, while the East is characterized by conductivity, which are also reflected in the horizontal slices. Conductors C1 and C2 extends to depth of 20 km and has no trap at the bottom, implying that they have a deep origin ([Bertrand et al., 2012](#)).

The middle and upper crust conductors C1 and C2 may originate from the upper mantle. [Wang S et al. \(2017\)](#) reveals that there are the conductors with approximately continuous distribution from the upper mantle to the middle and upper crust beneath the YGR, [Figure 1C](#). In addition, [Jin et al. \(2022\)](#) reveals the similar conductivity anomaly characteristics through sparse 3D magnetotelluric data. Due to large site spacing ($> 20 \text{ km}$), previous researches mainly reveal crust-mantle scale structures of YGR ([Lei et al., 2023](#)). On the contrary, the authors deployed the MT with site space of $\sim 0.6 \text{ km}$ in the GGF, which can reveal the fine electrical structure of the middle-upper crust. It is concluded that conductors C1 and C2 has a good spatial coupling relationship with the middle and lower crust conductors originating from upper mantle revealed by previous researches ([Figure 1C](#)), suggesting that they may have a high-temperature.

4 Discussion

4.1 Conductors C1 and C2 revealed by MT implying the heat source originating from mantle upwelling

Partial melting may contribute to the conductors C1 and C2 beneath the GGF. For active tectonic zones, the main mechanisms for generating conductors are partial melting and aqueous fluids ([Yang, 2011](#)). It may be more appropriate to interpret conductors C1 and C2 by partial melting ([Chen et al., 1996](#); [Unsworth et al., 2005](#)), because partial melting can continuously provide high terrestrial heat flow values ($\sim 100 \text{ mW/m}^2$, significantly higher than the surrounding areas, [Hu et al., 2000](#)) to the GGF. The resistivity revealed by MT can be used to estimate the fluid fraction ([Le Pape et al., 2015](#)). Partial melting zones may exist below C1 and C2 at depths of $\sim 8 \text{ km}$, with resistivity values of about $30 \Omega\text{m}$, indicating the presence of 2%–5% partial melting ([Gaillard and Marziano, 2005](#)). High-temperature and high-pressure experiments show that a small amount of water can affect partial melting fraction ([Yang, 2011](#)). The minor difference of resistivity between C1 and C2 may be due to the difference of water content in partial melting ([Holtz et al., 2001](#)).

Partial melting may originate from tearing of Indian slab (IS). The IS subducted beneath the Tibet at different angles (gentle in the west and steep in the east, [Liang and Song, 2006](#); [Li et al., 2008](#); [Zhao J et al., 2010](#); [Shi et al., 2020](#)). Since the uneven gravitational field of IS triggering the differential dragging, it gives rise to the tearing of IS into multiple pieces ([Chen et al., 2015](#); [Li and Song, 2018](#)). Mantle hot materials upwelled into the crust along the IS tearing windows and are geophysically imaged as low velocity bodies or high conductivity bodies in the middle and lower crust ([Nelson, 1996](#); [Wei et al., 2001](#); [Unsworth et al., 2005](#); [Jin et al., 2022](#)). In addition, the tearing of IS caused the East-West extension of the upper crust, and several North-South trending rifts were formed in the Southern Tibet, such as the YGR ([Wang Y et al., 2022](#); [Lei et al., 2023](#)). Mantle upwelling brought a large number of hot materials to the middle and lower crust ([Li and Song, 2018](#)), which lead to partial melting of crust. Partial melting of the middle and lower crust would penetrate the middle and upper crust along the tensile faults, forming the deep heat source of GGF. They are imagined as conductors C1 and C2 by MT ([Figures 5H, I](#)), which may be the origin of high terrestrial heat flow in the YGF. They are also supported by other evidences, such as seismic wave velocity ([Tian et al., 2015](#); [Wu et al., 2019](#); [Shi et al., 2020](#)), mantle CO_2 emission ([Kapp and Guynn, 2004](#); [Zhang et al., 2021](#)). Therefore, it is suggested that partial melting is the heat source driving high-temperature geothermal system of GGF, confirming the previous conjecture that heat source exists in the middle and upper crust ([Dorji, 2003](#); [Li and Hou, 2005](#); [Gao et al., 2022](#); [Wang R et al., 2022](#)).

4.2 Shallow geothermal system revealed by the AMT

The north-south normal fault is an important channel for fluid migration. In the GGF, the east-dipping active normal fault is a part

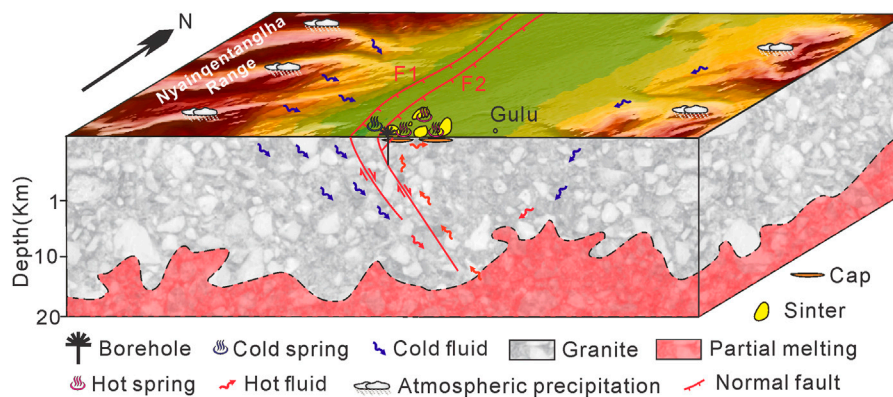


FIGURE 6

Cartoon model of geothermal system in Gulu geothermal field. Atmospheric precipitation feeds the underground fluids. The cold and hot fluids mainly migrate along the faults F1 and F2, respectively. The hydrothermal alteration zones below ~30–50 m of surface revealed by boreholes are the cap of geothermal system of Gulu geothermal field. Partial melting in middle and upper crust drives the geothermal system.

of the Nyainqentanglha fault, which undertakes the east-west stretching (~6 mm/yr) and triggered the 1952 Mw7.4 Gulu earthquake (Tapponnier et al., 1981; Armijo et al., 1986; Chevalier et al., 2020), laying the foundation for the development of hot springs (Gao et al., 2022). The ages of fault and sinters overlap since Miocene, suggesting a strong correlation between fault and geothermal fluids (Shen, 1992; Zhao Y et al., 2010). The five geothermal reservoirs and hidden geothermal alteration zones revealed by borehole ZK101 in the middle of GGF, suggesting that fault F2 is a geothermal fluid channel (Gao et al., 2022). The geothermal system elements, such as hot springs at the surface with high conductivity and geothermal reservoirs at the depth with high resistivity, are well imagined by AMT, Figures 3, 4, which are consistent with high-temperature geothermal systems worldwide (Ussher et al., 2000). Due to the low permeability and high resistivity of granite (Newman et al., 2008), geothermal reservoirs ($n \times 100 \Omega\text{m}$) tend to have higher resistivity than geothermal alteration zones (1–10 Ωm) (Wright et al., 1985; Pellerin et al., 1996; Piña-Varas et al., 2014). Based on such features, we believe that the yellow arrows in Figure 4 may represent geothermal reservoirs, and the fault F2 may be the upward migration channel of geothermal fluids.

Hydrothermal alteration zones, as the cap of geothermal system, seal off the hot fluids. Due to clays and brines, the hydrothermal alteration zones are often characterized by high conductivity (Wright et al., 1985; Muñoz, 2014). Horizontal resistivity slice of depth at 95 m shows that there is a large area of shallow conductors in GGF, Figure 3A. Not all conductors are the hydrothermal alteration zones (Muñoz, 2013). Fortunately, thermometer borehole can directly reveal the existence of hydrothermal alteration zone. Except for the thermometer boreholes below 50°C in Figure 3B, all the other boreholes reveal that there are hydrothermal alteration zones with a thickness of ~20–40 m distributed below 10 m on the surface, constituting the cap of the GGF geothermal system. In addition, the cold fluid migration is also worth identifying.

Fault F1 may be the channel for cold fluid migration. Fissures generated by faulting are important channels for surface fluids to

migrate to the depth (Dorji, 2003). On the horizontal slices, the conductors (C11–C14) with increasing depth clearly show that the migration pathways of cold fluids are converging from the periphery to the middle (Figures 3D,E), which are consistent with the topographic relief of GGF (Figure 3C). The resistivity models A2 and A3 indicate that the fluids in the east may not be deeply circulating, while the conductor C12 in the west may indicate deep circulation of fluids (Figure 4). In general, high-temperature geothermal reservoirs can only be formed through deep circulation of fluids (Cumming and Mackie, 2010; Muñoz, 2014). Hydrogen and oxygen isotopes reveal that atmospheric precipitation is an important supply source of underground fluids (Zhang et al., 1995; Liu et al., 2014). Some of them migrate deeply into the West of Nyainqentanglha range, and the others overflow to the surface on the east side of fault F1 in the form of cold spring (Figure 3A). The fluids with deep migrating have the characteristics of high conductivity, which is imaged as conductor C12 by AMT, Figures 4C, E. Therefore, it is suggested that fault F1 may be an important channel for the deep migration of cold fluids.

4.3 Implications for the geothermal system in the Gulu geothermal field

Conventionally, an ideal high-temperature geothermal system (temperature above 150°C–200°C, Muffler and Cataldi, 1978; Benderitter and Cormy, 1990) consists of heat source, heat reservoirs and cap, which are disputed in the tectonic active zones, such as plate boundaries, volcanic zones and rift zones (Majorowicz and Grasby, 2010; Muñoz, 2014). Conductive alteration cap overlying a more resistive reservoir is the classical electrical structure in the high-temperature geothermal systems, such as Taupo volcanic zone in New Zealand, Basin and Range province in California (Heise et al., 2007; Newman et al., 2008). The partially molten magma chambers are believed to be the heat source driving the geothermal systems (Wannamaker et al., 2004). Similar electrical structure and heat source also appear in the GGF. Unlike

them, the electrical structure in the GGF appears to be shallower in the depth and higher in resistivity value, possibly due to young geothermal fluids activity. Based on above analyses, the authors establish the geothermal system model of GGF, [Figure 6](#).

The atmospheric precipitation migrates to the depth along the normal fault F1. With the depth increases, these cold fluids are gradually heated by partial melting, and transform into high-temperature geothermal fluids. Due to the upward geothermal buoyancy ([Dorji, 2003](#)), the geothermal fluids begin to migrate upward along the normal fault F2, and form hot springs and geothermal alteration zones on the surface.

5 Conclusion

The Yadong-Gulu rift in southern Tibetan is a tensile active rift, which gives rise to high-temperature geothermal systems, and the Gulu geothermal field is located in its northern section. Through three-dimensional inversion of integrated magnetotelluric and audio magnetotelluric data, the electrical model of the Gulu geothermal field is obtained. MT and AMT imagine conductors (C11, C12 and C13 in shallow depth, C1 and C2 in the deep) and resistors (R11 and R1) beneath Gulu geothermal field. Combined with geology, boreholes and previous researches, this paper explains the conductors and resistors and obtains the following understandings.

- (1) Magnetotelluric reveals that conductors C1 and C2 are developed beneath the middle and upper crust of the Gulu geothermal field. The conductors may be the partial melting originating from the mantle upwelling, which drives the high-temperature geothermal system in the Gulu geothermal field.
- (2) Audio magnetotelluric reveals the shallow electrical structure of Gulu geothermal system. The hydrothermal alternation cap with high conductivity overlies the high-temperature geothermal reservoirs with high resistivity, which is consistent with the classical electrical structure of active rifts geothermal systems worldwide. Faults F1 and F2 may be the cold and hot fluids migration channels, respectively.
- (3) The geothermal system model of Gulu geothermal field constraining from the electrical structure is constructed. Cold fluids migrate from the periphery of Gulu geothermal field to the middle and supplies to the subsurface. Fault F1 may be the main downward migration channel of cold fluids. Due to the partial melting in the middle and upper crust, cold fluids are heated into hot fluids. Hot fluids may migrate upward along the

fault F2, forming a large number of thermal alteration zones and hot springs in the Gulu geothermal field.

Data availability statement

The raw data supporting the conclusion of this article will be made available by the authors, without undue reservation.

Author contributions

HW designed and organized the project. HW and QW analyzed the data. HW and QW interpreted the results and wrote the manuscript.

Funding

This research was partially supported by the Centralized R&D project of China National Nuclear Corporation ([2019] No. 419).

Acknowledgments

We thank Gary Egbert and Anna Kelbert for providing their 3D MT inversion code ModEM. We thank the associate editor and the reviewers for constructive comments that helped to improve this paper. We thank the researchers involved with collecting these valuable data. We are grateful to Shibing Xia for his assistance in mapping part of pictures.

Conflict of interest

The authors declare that this study received funding from China National Nuclear Corporation ([2019] No. 419). The funder had the following involvement in the study: design, data collection and analysis, decision to publish, and preparation of the manuscript.

Publisher's note

All claims expressed in this article are solely those of the authors and do not necessarily represent those of their affiliated organizations, or those of the publisher, the editors and the reviewers. Any product that may be evaluated in this article, or claim that may be made by its manufacturer, is not guaranteed or endorsed by the publisher.

References

- Abiye, T. A., and Haile, T. (2008). Geophysical exploration of the boku geothermal area, central Ethiopian rift. *Geothermics* 37, 586–596. doi:10.1016/j.geothermics.2008.06.004
- Armijo, R., Tapponnier, P., Mercier, J. L., and Han, T. L. (1986). Quaternary extension in Southern Tibet – field observations and tectonic implications. *J. Geophys. Res. Solid Earth* 91, 13803–13872. doi:10.1029/jb091ib14p13803
- Barbier, E. (2002). Geothermal energy technology and current status: An overview. *Renew. Sustain Energy Rev.* 6, 3–65. doi:10.1016/s1364-0321(02)00002-3
- Benderitter, Y., and Cormy, G. (1990). “Possible approach to geothermal research and relative costs,” in *Small geothermal resources: A guide to development and utilization*. Editors M. H. Dickson and M. Fanelli (New York: UNITAR), 59–69.
- Bertrand, E. A., Caldwell, T. G., Hill, G. J., Wallin, E., Bennie, S., Cozens, N., et al. (2012). Magnetotelluric imaging of upper-crustal convection plumes beneath the Taupo Volcanic Zone, New Zealand. *Geophys. Res. Lett.* 39, L02304. doi:10.1029/2011GL050177

- Bian, S., Gong, J., Zuza, A. V., Yang, R., Chen, L., Ji, J., et al. (2022). Along-strike variation in the initiation timing of the north-trending rifts in southern Tibet as revealed from the Yadong-Gulu rift. *Tectonics* 41, e2021TC007091. doi:10.1029/2021tc007091
- Chen, L. S., Booker, J. R., Jones, A. G., Wu, N., Unsworth, M. J., Wei, W. B., et al. (1996). Electrically conductive crust in southern Tibet from Indepth magnetotelluric surveying. *Science* 274 (5293), 1694–1696. doi:10.1126/science.274.5293.1694
- Chen, Y., Li, W., Yuan, X., Badal, J., and Teng, J. (2015). Tearing of the Indian lithospheric slab beneath southern Tibet revealed by SKS-wave splitting measurements. *Ear. Pla. Sci. Lett.* 413, 13–24. doi:10.1016/j.epsl.2014.12.041
- Chevalier, M., Taponnier, P., van der Woerd, J., Leloup, P. H., Wang, S., Pan, J., et al. (2020). Late Quaternary extension rates across the northern half of the Yadong-Gulu rift: Implication for east-west extension in southern Tibet. *Jour. Geoph. Res. Sol. Ear.* 125, e2019JB019106. doi:10.1029/2019JB019106
- Cumming, W. (2009). Geothermal resource conceptual models using surface exploration data[C], *proceedings, 34th workshop on geothermal reservoir engineering*, 187. SGP-TR-: Stanford University, 1–6.
- Cumming, W., and Mackie, R. (2010). “Resistivity imaging of geothermal resources using 1D, 2D and 3D MT inversion and TDEM static shift correction illustrated by a glass mountain case history,” in proceedings of world geothermal congress 2010, Bali, Indonesia, 25–29 April.
- Dorji, X. (2003). The basic characteristics of the yangbajing geothermal field— a typical high-temperature geothermal system. *China Eng. Sci.* 5 (1), 42–47. doi:10.3969/j.issn.10091742.2003.01.008
- Egbert, G. (2012). Hybrid conjugate gradient-Occam algorithms for inversion of multi-frequency and multi-transmitter EM data. *Geophys. J. Int.* 190, 255–266. doi:10.1111/j.1365-246x.2012.05523.x
- Egbert, G. (1997). Robust multiple-station magnetotelluric data processing. *Geophys. J. Int.* 130, 475–496. doi:10.1111/j.1365-246x.1997.tb05663.x
- Feng, Z., Zhao, Y., Zhou, A., and Zhang, N. (2012). Development program of hot dry rock geothermal resource in the Yangbajing Basin of China. *Renew. energy* 39 (1), 490–495. doi:10.1016/j.renene.2011.09.005
- Gaillard, F., and Marziano, G. I. (2005). Electrical conductivity of magma in the course of crystallization controlled by their residual liquid composition. *J. Geophys. Res.* 110, B06204. doi:10.1029/2004JB003282
- Gao, H., Hu, Z., Wan, H., Weilin, H., Song, Z., and Xiao, L. (2022). Characteristics of geothermal geology of the Gulu geothermal field in Tibet. Available at: <https://kns.cnki.net/kcms/detail/42.1874.P.20220506.0949.006.html>.
- Guo, Q. H., Wang, Y., and Wei, L. (2007). Major hydrogeochemical processes in the two reservoirs of the Yangbajing geothermal field, Tibet, China. *Jour. Vol Geo. Res.* 166 (3–4), 255–268. doi:10.1016/j.jvolgeores.2007.08.004
- Heise, W., Bibby, H. M., Caldwell, T. G., Bannister, S. C., Ogawa, Y., Takakura, S., et al. (2007). Melt distribution beneath a young continental rift: The Taupo volcanic zone, New Zealand. *Geophys. Res. Lett.* 34, L14313. doi:10.1029/2007GL029629
- Holtz, F., Johannes, W., Tamic, N., and Behrens, H. (2001). Maximum and minimum water contents of granitic melts generated in the crust: A reevaluation and implications. *Lithos* 56 (1), 1–14. doi:10.1016/S0024-4937(00)00056-6
- Hu, S. B., He, L., and Wang, J. (2000). Heat flow in the continental area of China: A new data set. *Ear. Plan. Sci. Lett.* 179 (2), 407–419. doi:10.1016/s0012-821x(00)00126-6
- Hu, Z. H., Gao, H. L., and Wan, H. P., (2022). Temporal and spatial evolution of hydrothermal alteration in the Yangbajing geothermal field, Tibet. *Geol. Rev.* 68 (1), 359–374. doi:10.16509/j.georeview.2021.12.105
- Jin, S., Sheng, Y., Comeau, M. J., Becken, M., Wei, W., Ye, G., et al. (2022). Relationship of the crustal structure, rheology, and tectonic dynamics beneath the Lhasa-Gangdese terrane (southern Tibet) based on a 3-D electrical model. *J. Geophys. Res. Solid Earth* 127, e2022JB024318. doi:10.1029/2022JB024318
- Kapp, P., and Guynn, J. H. (2004). Indian punch rifts Tibet. *Geology* 32, 993. doi:10.1130/g20689.1
- Kelbert, A., Meqbel, N., Egbert, G., and Tandon, K. (2014). ModEM: A modular system for inversion of electromagnetic geophysical data. *Comput. Geosciences* 66, 40–53. doi:10.1016/j.cageo.2014.01.010
- Le Pape, F., Jones, A. G., Unsworth, M. J., Vozar, J., Wei, W., Jin, S., et al. (2015). Constraints on the evolution of crustal flow beneath northern Tibet. *Geochem. Geophys. Geosystems* 16 (12), 4237–4260. doi:10.1002/2015GC005828
- Lei, L., Jin, S., Dong, H., Wei, W., Ye, G., and Zhang, L. (2023). 3-D electrical structure and tectonic dynamics in the Yangbajing area based on the array magnetotelluric data. *Front. Earth Sci.* 10, 1089675. doi:10.3389/feart.2022.1089675
- Li, C., van der Hilst, R. D., Meltzer, A. S., and Engdahl, E. R. (2008). Subduction of the indian lithosphere beneath the Tibetan plateau and Burma. *Ear. Plan. Sci. Lett.* 274 (1–2), 157–168. doi:10.1016/j.epsl.2008.07.016
- Li, J. T., and Song, X. D. (2018). Tearing of Indian mantle lithosphere from high-resolution seismic images and its implications for lithosphere coupling in southern Tibet. *Proc. Natl. Acad. Sci.* 115 (33), 8296–8300. doi:10.1073/pnas.1717258115
- Li, Z., and Hou, Z. (2005). “Partial melting in the upper crust in southern Tibet: Evidence from active geothermal fluid system,” in *Mineral deposit research: Meeting the global challenge* (Berlin, Heidelberg: Springer). doi:10.1007/3-540-27946-6317
- Liang, C., and Song, X. (2006). A low velocity belt beneath northern and eastern Tibetan Plateau from Pn tomography. *Geophys. Res. Lett.* 33, L22306. doi:10.1029/2006GL027926
- Liao, Z. (2017). *Thermal springs and geothermal energy in the qinghai-Tibetan plateau and the surroundings*. Springer, Berlin, Heidelberg. doi:10.1007/978-981-10-3485-5
- Liu, J., Shen, X. H., and Meng, K. (2009). Preliminary study on late Quaternary activity of faults in the Western margin of Gulu Basin. *Earthquake* 29 (3), 45–53. doi:10.3969/j.issn.10003274.2009.03.006
- Liu, Z., Lin, W., and Zhang, M. (2014). Origin of geothermal fluid and contribution of mantle source in Nimu-Nagqu, Tibet. *Earth Sci. Front.* 21 (6), 356–371. doi:10.13745/j.esf.2014.06.034
- Majorowicz, J., and Grasby, S. (2010). Heat flow, depth-temperature variations and stored thermal energy for enhanced geothermal systems in Canada. *J. Geophys. Eng.* 7 (3), 232–241. doi:10.1088/1742-2132/7/3/002
- Muffler, P., and Cataldi, R. (1978). Methods for regional assessment of geothermal resources. *Geothermics* 7, 53–89. doi:10.1016/0375-6505(78)90002-0
- Muñoz, G. (2014). Exploring for geothermal resources with electromagnetic methods. *Sur. Geo.* 35, 101–122. doi:10.1007/s10712-013-9236-0
- Nelson, K. D., Zhao, W., Brown, L. D., Kuo, J., Che, J., Liu, X., et al. (1996). INDEPTH seismic team Partially molten middle crust beneath southern Tibet: Synthesis of project INDEPTH results. *Science* 274, 1684–1688. doi:10.1126/science.274.5293.1684
- Newman, G., Gasperikova, E., Hoversten, G., and Wannamaker, P. E. (2008). Three-dimensional magnetotelluric characterization of the Coso geothermal field. *Geothermics* 37, 369–399. doi:10.1016/j.geothermics.2008.02.006
- Paolo, F., Ledo, J., Slazak, K., Martinez, D., Cabrera-Perez, I., and Perez, N. (2020). La Palma island (Spain) geothermal system revealed by 3D magnetotelluric data inversion. *Sci. Rep.* 10, 18181. doi:10.1038/s41598-020-75001-z
- Peacock, J. R., Thiel, S., Reid, P., and Heinson, G. (2012). Magnetotelluric monitoring of a fluid injection: Example from an enhanced geothermal system. *Geophys. Res. Lett.* 39, 1–5. doi:10.1029/2012gl053080
- Pellerin, L., Johnston, J. M., and Hohmann, G. W. (1996). A numerical evaluation of electromagnetic methods in geothermal exploration. *Geophysics* 61, 121–130. doi:10.1190/1.1443931
- Piña-Varas, P., Ledo, J., Queralt, P., Marcuello, A., Bellmunt, F., Hidalgo, R., et al. (2014). 3-D magnetotelluric exploration of Tenerife geothermal system (Canary islands, Spain), *Surv. Geophys.* 35:1045–1064 Nonlinear conjugate gradients algorithm for 2-D magnetotelluric inversion. *Geophysics* 66, 174–187. doi:10.1190/1.1444893
- Rybach, L. (2010). *Status and prospects of geothermal energy*. Bali, Indonesia: world geothermal congress.
- Shen, M. (1992). *Evolution and model of Yangbajing hydrothermal system. Selected papers of international symposium on high-temperature geothermal development and utilization in Tibet*, Lhasa, 95–98.
- Shi, D., Klemperer, S. L., Shi, J., Wu, Z., and Zhao, W. (2020). Localized foundering of Indian lower crust in the India-Tibet collision zone. *Proc. Natl. Acad. Sci.* 117, 24742–24747. doi:10.1073/pnas.2000015117
- Siripunvaraporn, W. (2011). Three-dimensional magnetotelluric inversion: An introductory guide for developers and users. *Surv. Geophys.* 33 (1), 5–27. doi:10.1007/s10712-011-9122-6
- Spycher, N., Peiffer, L., Sonnenthal, G. L., Saldi, G., Reed, M., and Kennedy, B. (2014). Integrated multicomponent solute geothermometry. *Geothermics* 51, 113–123. doi:10.1016/j.geothermics.2013.10.012
- Su, J., Tan, H., and Chen, X. (2020). The groundwater deep circulation and large-scale geothermal deposition in response to the extension of the Yadong-Gulu rift, South Tibet, China. *J. Volcanol. Geotherm. Res.* 395 (4), 106836. doi:10.1016/j.jvolgeores.2020.106836
- Taponnier, P., Mercier, J. L., Armijo, R., Han, T., and Zhao, T. J. (1981). Field evidence for active normal faulting in Tibet. *Nature* 294, 410–414. doi:10.1038/294410a0
- Tian, X. B., Chen, Y., Tseng, T., Klemperer, S., Thybo, H., Liu, Z., et al. (2015). Weakly coupled lithospheric extension in southern Tibet. *Ear. Plan. Sci. Lett.* 430, 171–177. doi:10.1016/j.epsl.2015.08.025
- Unsworth, M. J., Jones, A., Wei, W., Marquis, G., Gokarn, S. G., and Spratt, J. E. (2005). Crustal rheology of the Himalaya and Southern Tibet inferred from magnetotelluric data. *Nature* 438 (7064), 78–81. doi:10.1038/nature04154
- Ussher, G., Harvey, C., Johnstone, R., and Anderson, E. (2000). Understanding resistivities observed in geothermal systems, *Proceedings world geothermal congress*, Kyushu-Tohoku, Japan.
- Wang, G., Wei, W., Ye, G., Jin, S., Jing, J., Zhang, L., et al. (2017). 3-D electrical structure across the Yadong-Gulu rift revealed by magnetotelluric data: New insights on the extension of the upper crust and the geometry of the underthrusting Indian lithospheric slab in southern Tibet. *Earth Plan. Sci. Lett.* 474, 172–179. doi:10.1016/j.epsl.2017.06.027

- Wang, R., Winberg, F., Zhu, D., Hou, Z. Q., and Yang, Z. M. (2022). The impact of a tear in the subducted Indian plate on the Miocene geology of the Himalayan-Tibetan orogen. *GSA Bull.* 134 (3-4), 681–690. doi:10.1130/b36023.1
- Wang, S., Chevalier, M., Pan, J., Bai, M., Li, K., Li, H., et al. (2020). Quantification of the late Quaternary throw rates along the Yadong rift, southern Tibet. *Tectonophysics* 790, 228545. doi:10.1016/j.tecto.2020.228545
- Wang, S., Lu, C., Nan, D., Hu, X., and Shao, J. (2017). Geothermal resources in Tibet of China: Current status and prospective development. *Environ. earth Sci.* 76, 239. doi:10.1007/s12665-017-6464-5
- Wang, Y., and Guo, Q. (2010). *The yangbajing geothermal field and the Yangyi geothermal field: Two representative fields in Tibet, China*. Bali, Indonesia: Proceedings World Geothermal Congress, 25–29.
- Wang, Y., Li, L., Wen, H., and Hao, Y. (2022). Geochemical evidence for the nonexistence of supercritical geothermal fluids at the Yangbajing geothermal field, southern Tibet. *J. Hydrology* 604, 127243. doi:10.1016/j.jhydrol.2021.127243
- Wannamaker, P. E., Rose, P. E., Doerner, W. M., Berard, B. C., McCulloch, J., and Nurse, K. (2004). "Magnetotelluric surveying and monitoring at the coso geothermal area, California, in support of the enhanced geothermal systems concept: Survey parameters and initial results," in *proceedings, 29th workshop on geothermal reservoir Engineering* (United States: Stanford University).
- Wright, P., Ward, S., Ross, H., and West, R. C. (1985). State of the art geophysical exploration for geothermal resources. *Geophysics* 50, 2666–2696. doi:10.1190/1.1441889
- Wu, C. L., Tian, X. B., Xu, T., Liang, X., Chen, Y., Taylor, M., et al. (2019). Deformation of crust and upper mantle in central Tibet caused by the northward subduction and slab tearing of the Indian lithosphere: New evidence based on shear wave splitting measurements. *Earth Plan. Sci. Lett.* 514, 75–83. doi:10.1016/j.epsl.2019.02.037
- Wu, Z., Ye, P., Barosh, P., and Wu, Z. (2011). The October 6, 2008 Mw 6.3 magnitude Damxung earthquake, Yadong-Gulu rift, Tibet, and implications for present-day crustal deformation within Tibet. *J. Asian earth Sci.* 40, 943–957. doi:10.1016/j.jseas.2010.05.003
- Wu, Z., Zhao, X., Wu, Z., et al. (2006). Quaternary geology and faulting in the Damxung-Yangbajain basin, southern Tibet. *Jour. Geome.* 12 (3), 3005–3315.
- Yang, X. (2011). Origin of high electrical conductivity in the lower continental crust: A review. *Surv. Geophys* 32, 875–903. doi:10.1007/s10712-011-9145-z
- Yin, A., and Harrison, T. (2000). Geologic evolution of the Himalayan-Tibetan orogen. *Ann. Rev. Ear. Plan. Sci.* 28, 211–280. doi:10.1146/annurev.earth.28.1.211
- Yu, X., Wei, Z., Wang, G., Ma, X., Zhang, T., Yang, H., et al. (2022). Hot spring gas geochemical characteristics and geological implications of the northern Yadong-Gulu Rift in the Tibetan Plateau. *Front. Earth Sci.* 10, 863559. doi:10.3389/feart.2022.863559
- Zhang, J., Quay, P. D., and Wilbur, D. O. (1995). Carbon isotope fractionation during gas-water exchange and dissolution of CO₂. *Geochim. Cosmochim. Acta* 59, 107–114. doi:10.1016/0016-7037(95)91550-d
- Zhang, M., Lin, W., Liu, Z., Liu, Z., Hu, X., and Wang, G. (2014). Hydrogeochemical characteristics and genetic model of Gulu high-temperature geothermal system in Tibet. *Jour. Chengdu Univ. Tech. (Sci. Tech. Ed.)* 41 (3), 382–392. doi:10.3969/j.jssn.16719727.2014.03.15
- Zhang, M., Zhang, Li., Zhao, W., Guo, Z., Xu, S., Sano, Y., et al. (2021). Metamorphic CO₂ emissions from the southern Yadong-Gulu rift, Tibetan Plateau: Insights into deep carbon cycle in the India-Asia continental collision zone. *Chem. Geo.* 584, 120534. doi:10.1016/j.chemgeo.2021.120534
- Zhao, J., Yuan, X., Liu, H., Kumar, P., Pei, S., Kind, R., et al. (2010). The boundary between the Indian and Asian tectonic plates below Tibet. *Natl. Acad. Sci.* 107 (25), 11229–11233. doi:10.1073/pnas.1001921107
- Zhao, P., Xie, E., and Duoji, X. (2002). Geochemical characteristics and geological significance of geothermal gases in Tibet. *Acta petro. Sin.* 18 (4), 539–550.
- Zhao, Y., Zhao, X., and Ma, Z. (2010). Chronology and significance of Gulu geothermal spring type cesium deposit in Xizang Province. *Acta Geol. Sin.* 84 (2), 211–220.